Harnessing fluctuations to discover dissipative evolution equations

Xiaoguai Li[a], Nicolas Dirr[b], Peter Embacher[c], Johannes Zimmer[d], Celia Reina[a,*]

[a]*Department of Mechanical Engineering and Applied Mechanics, University of Pennsylvania, Philadelphia, PA 19104, USA*
[b]*School of Mathematics, Cardiff University, Cardiff CF24 4AG, UK*
[c]*Mathematics Institute, University of Warwick, Coventry CV4 7AL, UK*
[d]*Department of Mathematical Sciences, University of Bath, Bath BA2 7AY, UK*

Abstract

Continuum modeling of dissipative processes in materials often relies on strong phenomenological assumptions, as their derivation from underlying atomistic/particle models remains a major long-standing challenge. Here we show that the continuum evolution equations of a wide class of dissipative phenomena can be numerically obtained (in a discretized form) from fluctuations via an infinite-dimensional fluctuation-dissipation relation. A salient feature of the method is that these continuum equations can be fully pre-computed, enabling macroscopic simulations of arbitrary admissible initial conditions, without the need of any further microscopic simulations. We test this coarse-graining procedure on a one-dimensional non-linear diffusive process with known analytical solution, and obtain an excellent agreement for the density evolution. This illustrative example serves as a blueprint for a new multiscale paradigm, where full dissipative evolution equations — and not only parameters — can be numerically computed from lower scale data.

Keywords: Multiscale, Non-equilibrium thermodynamics, Fluctuation-dissipation, Coarse-graining

1. Introduction

Dissipative processes abound in material behavior and include, for instance, vacancy diffusion, dislocation mediated plasticity or phase transformations. Yet, their modeling and simulation face a deep gulf between macroscopic continuum models that are efficiently computable, although typically riddled with phenomenology, and lower scale atomistic/particle simulations, which are of higher physical fidelity, yet often exceedingly costly for real-life applications. Bridging this gulf has been a major research endeavor, which has spanned many disciplines, e.g., mechanics, mathematics or physics, and has lead to numerous coarse-graining strategies. Some prominent examples to determine the macroscopic evolution include concurrent and sequential multiscale techniques (Tadmor and Miller, 2011; Abdulle et al., 2012; Kevrekidis and Samaey, 2009), methods based on projection operators (Öttinger, 2005), and information-theoretic strategies (Machta et al., 2013); see also (Givon et al., 2004) for a review of mathematical approaches. However, few rigorous results are available, notably from hydrodynamic limit theory (Kipnis and Landim, 1999) or strategies as in Bodineau et al. (2016). This topic belongs to the vast field of macroscopic evolution discovery, for example via dimension reduction (Stephens et al., 2011; Daniels and Nemenman, 2015) and machine learning techniques (Rudy et al., 2017; Raissi, 2018), just to mention a few recent approaches.

Despite the numerous efforts, obtaining standalone continuum models (i.e., without concurrent lower scale simulations) that encode atomistic fidelity remains a major challenge. We present here a first step in this direction, by providing a coarse-graining methodology that numerically computes the macroscopic evolution operator of dissipative processes from the underlying field fluctuations. The methodology, which is sketched in Fig. 1 for a mass diffusion problem, presents three main attractive features. Firstly, the evolution operator can be completely pre-computed, enabling continuum simulations that do not require

*creina@seas.upenn.edu, dirrnp@cardiff.ac.uk, J.Zimmer@bath.ac.uk

concurrent atomistic calculations. Secondly, the method presented here computes the operator fully—not only parameters—and does not require a library of pre-existing operators. Thirdly, the computation of the operator only requires the fluctuations of the macroscopic fields (e.g., density fluctuations for the case of mass diffusion), which could in principle be determined experimentally. The first feature distinguishes this approach from existing multiscale techniques, while the second one differentiates it from machine learning approaches.

We further emphasize that the proposed strategy does not prescribe *a priori* (phenomenologically) the closed-form equation for the macroscopic evolution; yet, it is not an equation-free method. More specifically, the goal of equation-free calculations is to circumvent the difficulties underlying continuum modeling, and directly evolve the macroscopic fields by computing their time derivatives from concurrent microscopic simulations over small spatio-temporal domains. The macroscopic simulations are then carried over larger spatio-temporal intervals leading to large efficiency savings as compared to fully resolved microscopic simulations: for 10^8 random walkers (independent particles) on a one-dimensional domain, simulations using equation-free techniques are by a factor of 1000 faster than direct Kinetic Monte Carlo simulations (Erban et al., 2006). In contrast, the multiscale methodology we propose in this paper seeks to numerically extract the macroscopic equations from atomistic data, and to do so at a pre-calculation stage. This allows to perform macroscopic simulations without the need of further atomistic calculations, thus avoiding the biggest computational cost factor in equation-free methods or other concurrent multiscale strategies: the bursts of microscopic simulations during run time. For example, the one-dimensional particle simulations described below (approximately 35 000 particles undergoing a diffusive process) for the full time interval of interest would take several days, while the computational cost of the macroscopic simulations with the model obtained by the method presented here — based on a finite element discretization — gets reduced to essentially no computation time (after the pre-calculation stage), while maintaining physical fidelity of the underlying particle model.

In its current form, the proposed coarse-graining strategy applies to purely dissipative processes, that is, those not coupled to reversible phenomena, such as elastic deformations. We further require that the underlying atomistic/particle system is in local equilibrium with Gaussian fluctuations (this will be made precise later). A prototypical example of a purely dissipative process is particle diffusion, which is ubiquitous in solids at high temperatures and central to microstructure evolution and material properties (Mehrer, 2007). The extension of the present approach to account for reversible phenomena is a natural next step

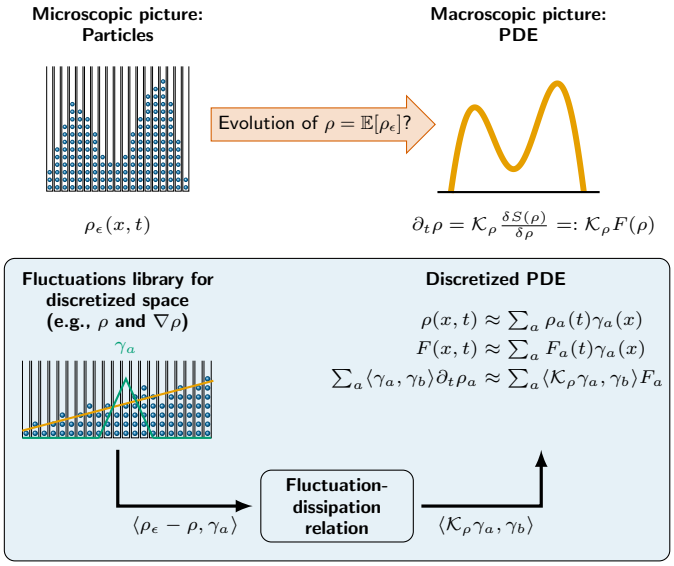

Figure 1: Sketch of the proposed computational strategy to determine the dissipative operator $\mathcal{K}$ in discretized form, using basis functions $\{\gamma(x)\}$, for the specific case of a density field ρ.

and will be pursued in future investigations. In this regard, we refer the reader to Mielke (2011) for the thermodynamic structure of a wide range of material models with reversible and irreversible components (e.g., thermoelasticity or viscoelasticity) as well as purely dissipative ones (e.g., phase field models).

A central element of the strategy is a novel infinite-dimensional fluctuation-dissipation statement, which generalizes existing finite-dimensional results. The latter have been widely used to determine transport coefficients (i.e., parameters in otherwise fully specified operators, such as diffusivity) (Green, 1954; Kubo, 1966; Marconi et al., 2008; Embacher et al., 2018). In contrast, the new approach allows us to infer the evolution operator (including parameters therein) by probing fluctuations systematically.

We here exemplify the coarse-graining procedure for one of the few particle processes for which the macroscopic evolution may be computed analytically, namely a one-dimensional zero-range process whose continuum limit obeys a non-linear diffusion equation. The results indicate an excellent agreement for the density evolution of various initial profiles, and the errors between the numerical and analytical operators are quantified.

The paper is organized as follows. In Section 2, we introduce the class of systems to which the methodology applies as well as the infinite-dimensional fluctuation-dissipation relation which underpins the coarse-graining strategy. Section 3 describes the numerical procedure, and Section 4 exemplifies the approach for a diffusive particle system. Finally, conclusions are provided in Section 5.

2. Outline of the approach

Underlying the proposed strategy is the assumption that macroscopic dissipative evolutions in 'thermodynamic' form can be written as

$$\partial_t z = \mathcal{K}(z)\frac{\delta S(z)}{\delta z} =: \mathcal{K}_z \frac{\delta S(z)}{\delta z}, \tag{1}$$

where $z = z(x,t)$ is the field of interest, S is the entropy of the system, $\frac{\delta S(z)}{\delta z}$ its variational derivative and $\mathcal{K}_z$ is a symmetric positive semi-definite linear operator; we write $\mathcal{K}_z$ to emphasize that $\mathcal{K}$ depends on z. On the level of nonequilibrium thermodynamics/mechanics, (1) describes a wide range of evolution equations.

The specific question addressed in this paper is the following: given a particle model that leads, in a suitable scaling limit of infinitely many particles, to an equation of the form (1), how can we determine the operator $\mathcal{K}_z$ purely from the observation of finitely many particles? We focus on $\mathcal{K}_z$ since the computation of $\frac{\delta S(z)}{\delta z}$ can, in many situations, be accomplished by free energy computations (Lelièvre et al., 2010).

The key observation is that the evolution of a large, yet *finite* number of particles, can often be formally described by a stochastic partial differential equation of the form

$$\partial_t z_\epsilon = \mathcal{K}_{z_\epsilon}\frac{\delta S(z_\epsilon)}{\delta z_\epsilon} + \sqrt{\epsilon}\sqrt{2\mathcal{K}_{z_\epsilon}}\dot{W}_{x,t}, \tag{2}$$

where $\dot{W}_{x,t}$ is a space-time white noise, $\mathbb{E}\left[\dot{W}_{x,t}\dot{W}_{y,s}\right] = \delta(x-y)\delta(s-t)$, and the equation is to be interpreted in a weak formulation. This is the fluctuating hydrodynamics equation associated with (1), for diffusive systems (Eyink, 1990, Section 6), (Eyink et al., 1996, Section 4), or those described by an additive noise. It encodes an infinite-dimensional fluctuation-dissipation relation $\sigma_z\sigma_z^* = 2\epsilon\mathcal{K}_z$, with the fluctuation operator $\sigma_z = \sqrt{\epsilon}\sqrt{2\mathcal{K}_{z_\epsilon}}$ acting on the noise. Its finite dimensional counterpart has long being used to extract transport coefficients. See, for example, the monographs (Stratonovich, 1992; Zwanzig, 2001; Klages et al., 2013), and the articles (Eyink et al., 1996, Section 3), (Maes, 1999) for fluctuation-dissipation relations.

As a simple example of (2), the evolution of N random walkers X_i on a lattice described by $\rho_\epsilon := \frac{1}{N}\sum_{i=1}^N \delta_{X_i}$ is given by an equation of Dean type (Dean, 1996) ($N = C/\epsilon$, ϵ being the individual lattice site volume and C a constant)

$$\partial_t \rho_\epsilon = \operatorname{div}(D\nabla\rho_\epsilon) + \sqrt{\epsilon}\operatorname{div}(\sqrt{2D\rho_\epsilon}\dot{W}_{x,t}). \tag{3}$$

This equation is of the form (2), with $S(\rho) = -\int \rho\log(\rho)\,\mathrm{d}x$ being the Boltzmann entropy in dimensionless units and $\mathcal{K}_\rho$ the operator $\mathcal{K}(\rho)\xi = -\operatorname{div}(D\rho\nabla\xi)$; see Reina and Zimmer (2015) for the calculation of $\sqrt{\mathcal{K}_\rho}$

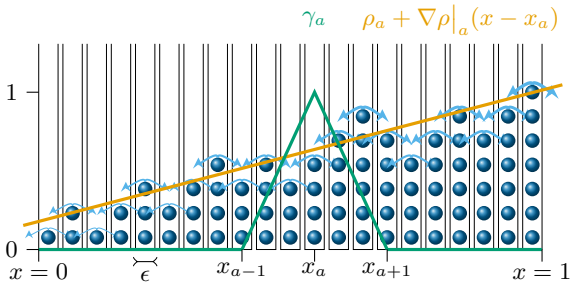

Figure 2: Sketch of a profile $\rho_a + \nabla\rho|_a(x - x_a)$ simulated to measure density fluctuations, and a basis function γ_a. The jump rate for each lattice site increases with the number of particles, as indicated by the thickness of the arrows.

in this case (note that Dean derives an equation for $\sum_{i=1}^{N} \delta_{X_i} = N\rho_\epsilon(x)$, which is why the noise in Dean (1996) differs from the one in (3) by a factor of $\sqrt{N}$; this difference in scaling is crucial, see (Eyink, 1990, Section 6)). There is a wide range of applications of (2) and its extension to account for reversible phenomena, for example, phase field models Castro (2003), nonequilibrium bacterial dynamics (Thompson et al., 2011, Eq. (71)), nucleation theory (Lutsko, 2012, Eqs. (8) and (20)) and liquid film theory (Grün et al., 2006, Eq. (19)); see (Durán-Olivencia et al., 2017) for connections to dynamic density functional theory.

3. Numerical procedure

We now show that the fluctuation-dissipation relation in (2) can be harnessed to numerically compute a discretized version of the operator $\mathcal{K}_z$ from particle data. More specifically, we consider an approximation of the macroscopic field z and its associated thermodynamic force $F := \delta S/\delta z$ of the form $z(x,t) \approx \sum_a z_a(t)\gamma_a(x)$ and $F(x,t) \approx \sum_a F_a(t)\gamma_a(x)$, where $\{\gamma_a\}$ is a suitable basis of functions. The weak form of the evolution equation (1) then reads

$$\sum_a \langle \gamma_a, \gamma_b \rangle \partial_t z_a = \sum_a \langle \mathcal{K}_z \gamma_a, \gamma_b \rangle F_a, \text{ for all } b, \tag{4}$$

where $\langle , \rangle$ denotes the L^2 inner product, and the matrix $\langle \mathcal{K}_z\gamma_a, \gamma_b\rangle$ represents a discretization of the unknown operator. In analogy to the quadratic variation formula for the stochastic ODE $\mathrm{d}X = f\,\mathrm{d}t + \sqrt{\sigma}\,\mathrm{d}W_t$ in dimension n, where

$$\sigma = \lim_{h \searrow 0} \frac{1}{hn} \mathbb{E}\left[[X(t_0 + h) - X(t_0)]^2 \right],$$

the element $\langle \mathcal{K}_z\gamma_a, \gamma_b\rangle$ can be related to the covariation of the rescaled local fluctuations as

$$\langle \mathcal{K}_z \gamma_a, \gamma_b \rangle = \lim_{h \searrow 0} \frac{1}{2h} \mathbb{E}\Big[\left(Y_{\gamma_a}(t_0 + h) - Y_{\gamma_a}(t_0)\right) \cdot \left(Y_{\gamma_b}(t_0 + h) - Y_{\gamma_b}(t_0)\right) \Big], \tag{5}$$

where Y_γ is the limit of $\langle z_\epsilon - z, \gamma\rangle/\sqrt{\epsilon}$ and $z = \mathbb{E}[z_\epsilon]$. The proof of this statement can be found in Appendix B. It uses mathematical arguments similar to Embacher et al. (2018), but extends the result considerably: now the entire operator can be characterized, while in Embacher et al. (2018) only one parameter (the diffusivity) could be extracted for an otherwise fully prescribed operator.

Relation (5) enables the calculation of the discretized operator $\mathcal{K}_z$ from particle fluctuations. However, the result is, in general, profile dependent, as indicated by the subscript z in $\mathcal{K}_z$, and thus the argument z is still infinite-dimensional. This is another key difference to Embacher et al. (2018), where the diffusivity depends on a scalar density value. Therefore additional arguments are required to pre-compute the operator. Namely, we consider functions γ with local support and assume that $\mathcal{K}_z$ is a local and regular operator, such that a Taylor approximation in z can be employed (these assumptions are satisfied for a wide range of operators and suitable choices of z). Then, a numerical approximation of the left-hand side of (5) is

$$\langle \mathcal{K}_z \gamma_a, \gamma_b \rangle \approx \langle \mathcal{K}_{(z_a + \nabla z|_a (x - x_a) + \ldots)} \gamma_a, \gamma_b \rangle \tag{6}$$

for sufficiently high order of the Taylor expansion and suitable basis functions; here $z_a = z(x_a)$, where x_a the mid-point of γ_a, see Fig 2, and ∇ is the spatial gradient. We remark that the assumption of locality of the operator can be numerically probed, by evaluating $\langle \mathcal{K}_z \gamma_a, \gamma_b \rangle$ for functions γ_a and γ_b with non-overlapping support.

In practice, the calculation of $\langle \mathcal{K}_{(z_a + \nabla z|_a (x - x_a) + \ldots)} \gamma_a, \gamma_b \rangle$ in (6) as a function of $z_a, \nabla z|_a, \ldots$ is implemented for a discretized space V_{discr}, i.e., for finitely many values of $z_a, \nabla z|_a, \ldots$ within a prescribed range (see Fig. 2 for $z \coloneqq \rho$, and the space V given by ρ and $\nabla \rho$). This is obtained via (5) from particle data (finite ϵ), for small but finite h, and expectations are approximated as averages over R realizations. The resulting discrete operator is then interpolated in V to perform continuum simulations with (4) and (6), for arbitrary initial conditions and boundary data (here periodic or Dirichlet boundary conditions). Although the pre-calculation of $\mathcal{K}_z$ can be laborious, requiring a considerable number of simulations (of the order of $R \times$ size of the discrete space V_{discr}), these are trivially parallelizable and only executed over a small time interval. Moreover, once the operator is computed, the macroscopic simulations can be run without any further particle simulations.

4. Computational results

We now demonstrate the applicability of this coarse-graining strategy with an illustrative example, where the the analytical solution is known, and the errors may thus be quantified. Specifically, we consider a symmetric zero-range process (ZRP) in a one-dimensional lattice. Here, particles jump with a rate $g(k) = k^2$, where k is the occupation number of the specific site, see Fig. 2. This particle process can be efficiently simulated using a Lattice Kinetic Monte Carlo approach, and, in the limit of infinite number of particles ($\epsilon \to 0$), the density profile evolves according to the PDE

$$\begin{aligned} &\partial_t \rho = -\operatorname{div}\left(m(\rho) \nabla \frac{\delta S(\rho)}{\delta \rho} \right), \quad \text{with} \\ &\frac{\delta S}{\delta \rho} = F(\rho) = -\log\left(2m(\rho)\right), \text{ and } \rho(m) = \sqrt{2m}\frac{I_1\left(2\sqrt{2m}\right)}{I_0\left(2\sqrt{2m}\right)}, \end{aligned} \tag{7}$$

where I_i are the modified Bessel functions of the first kind; see (Grosskinsky et al., 2003; Embacher et al., 2018) for the derivation.

We choose linear finite element shape functions satisfying $\gamma_a(x_b) = \delta_{ab}$ (see Fig. 2), which lead to a tri-diagonal matrix for $\langle \mathcal{K}_\rho \gamma_a, \gamma_b \rangle$, and a linear approximation for ρ in $\mathcal{K}_\rho$. The discretized evolution equation for the density then reads (for all b)

$$\sum_a \langle \gamma_a, \gamma_b \rangle \partial_t \rho_a \approx \sum_{a \in \{b-1, b, b+1\}} \langle \mathcal{K}_{(\rho_a + \nabla \rho|_a (x - x_a))} \gamma_a, \gamma_b \rangle F_a; \tag{8}$$

we remark that this choice is an assumption made *a priori* on $\mathcal{K}_\rho$ and that it can in principle be generalized to higher-order elements and Taylor approximations. With these approximations, the discretized operator can be tabulated by means of three components ($a \in \{b-1, b, b+1\}$) which depend on ρ and $\nabla \rho$, and which can be computed for a discrete space V_{discr} from particle simulations. The probed space V_{discr} and the three non-zero entries (main, super- and sub-diagonals) of $\langle \mathcal{K}_{(\rho_a + \nabla \rho|_a (x - x_a))} \gamma_a, \gamma_b \rangle$ are plotted in Fig. 3, together with a polynomial fit that ensures mass conservation (i.e., the sum of the three entries being equal to zero); see Appendix A for further details on these calculations.

The resulting fitted operator in V can then be utilized to compute the continuum evolution for arbitrary initial profiles, via (8). We here use the analytical thermodynamic force, cf. (7), to probe the accuracy of the operator. Figure 4 shows two of such evolutions: the left figure depicts the time progression of a cosine initial profile with periodic boundary conditions, whose density and gradient lie within the bounds of the probed region in V, while the right figure considers a non-symmetric initial density with fixed Dirichlet data extrapolating beyond this region. The full temporal evolution in movie format can be displayed by clicking on the corresponding images (online version only – Movie1.mp4 and Movie2.mp4). The results

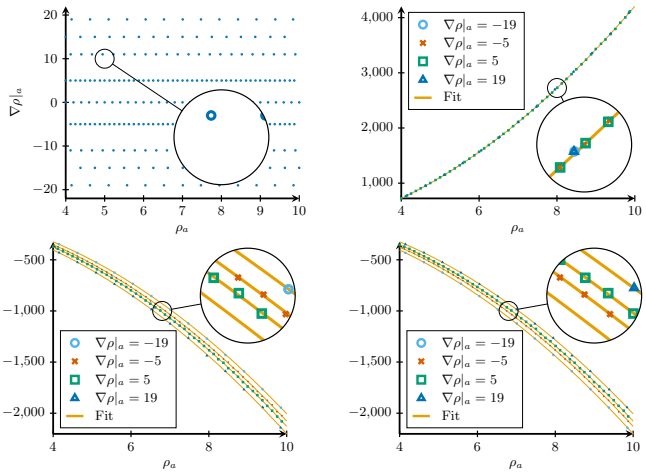

Figure 3: Top left: Discrete set V_{discr} of pairs $(\rho_a, \nabla\rho|_a)$ used to evaluate the discretized operator $\mathcal{K}_\rho$. Remaining plots: Shown are the matrix entries (b, a) of $\langle \mathcal{K}_{(\rho_a + \nabla\rho|_a (x - x_a))} \gamma_a, \gamma_b \rangle$ as function of ρ_a and $\nabla\rho|_a$ for a symmetric zero-range process. The plots are for $a = b$ (top right), $a = b - 1$ (bottom left) and $a = b + 1$ (bottom right). For x, x_a and the profiles γ_a see Fig. 2 in the main text.

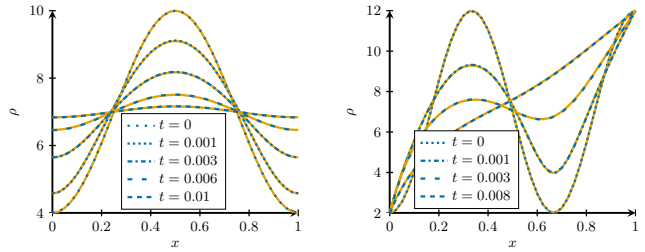

Figure 4: Comparisons between the particle-based solution (blue) and the solution to the PDE from (7) (orange) for different initial and boundary conditions. Left: Periodic boundary conditions. Right: Inhomogeneous Dirichlet data.

show an outstanding agreement between the particle-informed evolution and the solution of the PDE given explicitly by (7), with an identical spatio-temporal discretization scheme. A similar study without the mass conservation constraint is for comparison given in Appendix A. As it is there observed, results of good accuracy require an increase of the size of V_{discr} by more than an order of magnitude.

We further remark that the tabulated discrete operator can provide insight in its differential form, at least for simple cases. In particular, for the zero-range process studied, whose infinite particle limit satisfies the PDE $\partial_t \rho = -\operatorname{div}(m(\rho)\nabla F) = -m\Delta F - \nabla m \nabla F$, see (7), the discrete operator reveals a structure of the form

$$\begin{aligned} \langle \mathcal{K}_{(\rho_a + \nabla\rho|_a (x - x_a))} \gamma_a, \gamma_b \rangle &=: K_{ba}(\rho_a, \nabla\rho|_a) \\ &= K_{ba}^{(1)}(\rho_a) + K_{ba}^{(2)}(\rho_a, \nabla\rho|_a), \end{aligned} \tag{9}$$

where the ratio of the coefficients result in a stencil of $K_{ba}^{(1)}$ equal to $-1, 1.999936, -0.999936$ (i.e., these are the proportionality factors for the entries $a = \{b - 1, b, b + 1\}$ with b fixed), which may be identified with the Laplacian; and a stencil of $K^{(2)}$ equal to $-1, 0.003763, 0.996237$, which corresponds to the gradient. These stencils are obtained from the constrained fitting method, noting that the discretized operator is symmetric up to higher order terms. The structure of the right-hand side of the evolution equation is thus recovered.

The errors between the discrete operator obtained numerically from fluctuations and its continuum version arise from three sources: (i) the finite element discretization of the operator, (ii) the Taylor expansion in (8), and (iii) and its evaluation from particle fluctuations, including the interpolation scheme. The second

error source is examined in detail in Appendix C for the case of diffusion, while the first one can be analyzed in a standard way, and the third one has been numerically examined in (Embacher et al., 2018).

5. Conclusions and outlook

This is, to the best of our knowledge, the first time that a dissipative continuum equation has been numerically recovered from particles using a physics-based approach, in this case, an infinite-dimensional fluctuation-dissipation relation. We note that the required assumptions are only threefold: a particle process which, for finitely many particles, is described by (2), and is in local equilibrium with Gaussian fluctuations (see for example Landim (2002) and (Dirr et al., 2016, Section IV.B) for a precise mathematical formulation). The result is a sequential multiscale scheme that leads to (discretized) continuum evolution equations which are both efficiently computable and free of phenomenology, thus escaping the usual compromise between these two features in current computational multiscale techniques.

In this paper, we confined ourselves to problems where the macroscopic evolution is known analytically, which enables us to quantify the error of the numerically computed operator. Future work will address the application of the computational strategy developed here to systems with different evolution operators. A classical gradient flow dynamics different to the Wasserstein evolution studied here (i.e., weighted H^{-1} operator) is the one characterized by an L^2 operator. We note that H^{-1} and L^2 are the two most common evolution operators for microstructure evolution, see Carter et al. (1997); both are also standard in the modeling of a wide variety of physical phenomena. Their associated stochastic equations are often denoted as Model A and B, respectively (Hohenberg and Halperin, 1977), and have a structure analogous to (2), which is the cornerstone of the methodology here presented. Other evolution operators arise for instance in the Derrida-Lebowitz-Speer-Spohn (DLSS) equation, introduced by Derrida et al. (1991) to describe interface fluctuations in a spin system. It is also, in multidimensional form, a model for a quantum drift-diffusion in semiconductors. In d dimensions, it can be written as

$$\partial_t \rho = -\sum_{i,j=1}^{d} \partial_{ij}^2 \left(\rho \partial_{ij}^2 \log(\rho) \right), \tag{10}$$

which suggests that the operator associated with the entropy $S(\rho) = -\rho \log(\rho)$ is $\mathcal{K}\xi = \sum_{i,j=1}^{d} \partial_{ij}^2 \left(\rho \partial_{ij}^2 \xi \right)$. The examples above are situations where it is not sufficient to assume that the operator is of the form $\mathcal{K}_\rho \xi = -\operatorname{div}\left(m(\rho) \nabla \xi \right)$ and use mean square displacement or the approach of Embacher et al. (2018) to compute diffusion / mobility coefficients.

There are also many other systems for which the evolution operator is not known. Some of these examples include the diffusion of interacting particles (Vlachos and Katsoulakis, 2000), with short-range interactions, or processes with volume exclusion, where the operator is only presently known for certain parameter regimes (Bruna and Chapman, 2012). The analysis of these systems and related ones via the coarse-graining strategy described in this article is an area of future research.

In summary, the example studied here can serve as a blueprint for the study of a wider spectrum of dissipative phenomena, with applications ranging from multiparticle diffusion and phase transformations in solids, over chemotaxis in heterogeneous environment to protein diffusion in membranes. Such investigations should be complemented by a rigorous numerical analysis of convergence and rates. These questions are beyond the scope of the present study and will be the subject of future investigations.

Appendix A. Computational details for the zero-range process

In this section, we provide more information on the particle and continuum simulations for the zero-range process and compare the coarse-grained results where mass conservation is incorporated with results where this constraint is not imposed.

For the process considered, we evaluate the discretized operator $\langle \mathcal{K}_{(\rho_a + \nabla\rho|_a (x - x_a))} \gamma_a, \gamma_b \rangle$ using simulations with flat profiles with $\rho_a \in [4 : 0.1 : 10]$, and affine profiles with $\nabla\rho|_a \in \pm[5, 11, 15, 19]$, see Fig. 2 For

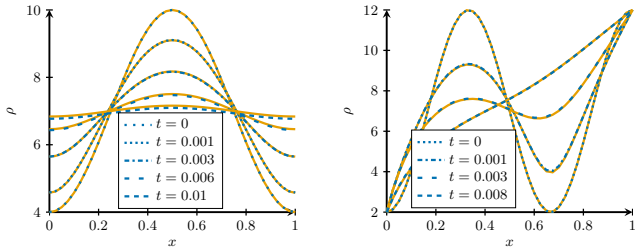

Figure A.5: Comparisons between the particle-based solution (blue) and the solution of the PDE from (7) (orange) for different initial and boundary conditions, not imposing mass conservation on the discretized operator. Left: Periodic boundary conditions. Right: Inhomogeneous Dirichlet data.

each of these profiles, $R = 800\,000$ realizations are performed over the unit interval as computational domain, with 5000 lattice sites ($\epsilon = 1/5000$). The system is first evolved over a time interval $t_0 - t_{\text{ini}} = 4.004 \times 10^{-6}$ to reach local equilibrium, and subsequently over a time interval $h = 4 \times 10^{-11}$, which is used for the calculation of the expectations. In practice, the equilibration time interval is much larger than h, yet macroscopically small, leading to negligible changes of the macroscopic profile. To save computational time, a method described in Embacher et al. (2018) is used to generate the multiple realizations (see also the pseudo-code in Algorithm 1 below). In addition, 40 equally spaced shape functions γ_a are considered. This results in 125 lattice sites within the support of each function γ_a that is fully contained in the computational domain. The resulting values of the matrix entries $\langle \mathcal{K}_{(\rho_a + \nabla\rho|_a (x - x_a))} \gamma_a, \gamma_b \rangle$ evaluated at specific points $(\rho_a, \nabla\rho|_a)$ in V_{discr} are then extended to V, via a suitable interpolation scheme. A naïve approach with an independent interpolation of the individual matrix components will in general, however, not lead to a mass preserving scheme, in contrast to what the particle process implies. Therefore, for the results of the main text, we imposed mass conservation in the fitting process by ensuring that the entries in each column sum up to 0. This is achieved using a least square fit with second order polynomials in $(\rho_a, \nabla\rho|_a)$ for each of the three matrix entries, the sum of which we enforce to vanish identically. Figure 3 shows the chosen discrete set V_{discr} and resulting entries for the operator, together with the polynomial fit. These were used to obtain Fig. 4, where all simulations employed an explicit time discretization scheme.

We remark that in the absence of the mass conservation constraint, good results can still be achieved as shown in Fig. A.5 (see also the corresponding movies by clicking on the images – online version only, Movie3.mp4 and Movie4.mp4), although small deviations may be observed at large times (see left panel). The discrete set V_{discr} used in these simulations is shown in Fig. A.6, together with the entries for the operator and their (independent) quadratic fit. To achieve the observed accuracy, a relatively large size of the set V_{discr} is required. Specifically, V_{discr} consists of 6111 points, in contrast to 228 points when mass conservation is imposed.

Algorithm 1 Pseudo-code describing the method in algorithmic form.

Begin

// Step 1: Zero range process simulation
// Set lattice domain and scaling:

$\epsilon = \frac{1}{L}$, $x_i = \frac{X_i}{L}$; // Spatial discretization with L lattice sites; X_i is the lattice coordinate

// Generate particle data from linear initial profile $\rho\left(t_{\text{ini}}L^2, X_i\right)$

: **for** *all* R_1 *realizations starting from* t_{ini} **do**

  $\rho_r\left(t_{\text{prep}}L^2, X_i\right) = \text{stochastic-evolution}\left(\left[t_{\text{ini}}, t_{\text{prep}}\right], \rho\left(t_{\text{ini}}L^2, X_i\right)\right)$;

  for *all* R_2 *realizations starting from* t_{prep} **do**

    $\rho_r\left(t_0L^2, X_i\right) = \text{stochastic-evolution}\left(\left[t_{\text{prep}}, t_0\right], \rho_r\left(t_{\text{prep}}L^2, X_i\right)\right)$;

    $\rho_r\left(\left(t_0+h\right)L^2, X_i\right) = \text{stochastic-evolution}\left(\left[t_0, t_0+h\right], \rho_r\left(t_0L^2, X_i\right)\right)$;

$R = R_1 \cdot R_2$; // Total number of realizations in $[t_0, t_0+h]$

$\rho\left(t_0, x_i\right) = \frac{1}{R} \cdot \sum_r \left(\rho_r\left(t_0L^2, X_i\right)\right)$; // Approx. deterministic state

$\rho\left(t_0+h, x_i\right) = \frac{1}{R} \cdot \sum_r \left(\rho_r\left(\left(t_0+h\right)L^2, X_i\right)\right)$;

// Step 2: Compute discrete operator using equation (5)
// Basis function γ_a with $a \in [1, N_\gamma]$:

$x_{\text{basis},a} = \frac{a}{N_\gamma}$ // Center of a^{th} basis function, γ_a

Function $\gamma_a\left(x_i\right)$

  $\gamma_a\left(x_i\right) = \max\left(0, 1 - N_\gamma|x_i - x_{\text{basis},a}|\right)$;

  return $\gamma_a\left(x_i\right)$;

for *all* R *realizations* r **do**

  for *all microscopic positions* X_i **do**

    $Y_{\gamma_a,r}\left(t_0\right) = \sqrt{\epsilon}\sum_i \left[\gamma_a(x_i)\left(\rho_r\left(t_0L^2, X_i\right) - \rho\left(t_0, x_i\right)\right)\right]$;

    $Y_{\gamma_a,r}\left(t_0+h\right) = \sqrt{\epsilon}\sum_i \left[\gamma_a(x_i)\left(\rho_r\left(\left(t_0+h\right)L^2, X_i\right) - \rho\left(t_0+h, x_i\right)\right)\right]$;

    $\rho_{a,r} = \frac{\sum_i \gamma_a(x_i)\rho_r\left((t_0+h)L^2, X_i\right)}{\sum_i \gamma_a(x_i)}$;

$K_{ba} = \frac{1}{2h}\frac{1}{R-1}\sum_r \left(Y_{\gamma_a,r}\left(t_0+h\right) - Y_{\gamma_a,r}\left(t_0\right)\right)\left(Y_{\gamma_b,r}\left(t_0+h\right) - Y_{\gamma_b,r}\left(t_0\right)\right)$;

// $\langle \mathcal{K}_\rho\gamma_a, \gamma_b\rangle = \frac{1}{2h}\mathbb{E}\Big[\left(Y_{\gamma_a}(t_0+h) - Y_{\gamma_a}(t_0)\right)\cdot\left(Y_{\gamma_b}(t_0+h) - Y_{\gamma_b}(t_0)\right)\Big]$

$\rho_a = \frac{1}{R}\sum_r \rho_{a,r}$;

// Step 3: Fit K_{ba} as a function of ρ_a and slope of initial profile $\nabla\rho_a$ with/without mass conservation constraint

// Step 4: Compute macroscopic evolution of initial profile $\rho_0(x)$
// Initialize $\langle\gamma_a, \gamma_b\rangle$ on the left hand side of Equation (4)

if *periodic boundary condition* **then**

  $M_{ab} = \langle\gamma_a, \gamma_b\rangle$, with periodic γ;

if *Dirichlet boundary condition* **then**

  $M_{ab} = \langle\gamma_a, \gamma_b\rangle$, with nonperiodic γ;

  $M_{uu} = M(2 : N_\gamma - 1, 2 : N_\gamma - 1)$; // partitioning of matrix M

$t = 0$;

Δt = time step;

T = total simulation time;

while $t<T$ **do**
  Compute analytic driving force $F_a(x_i)$;
  Build matrix $\langle \mathcal{K}_z \gamma_a, \gamma_b \rangle$ by $K_{ba} = K_{ba}(\rho_a(t), \nabla\rho_a(t))$;
  if *periodic boundary condition* **then**
    `// explicit solver`
    $\rho_{t+\Delta t} = \rho_t + \Delta t M^{-1} K F$; ; `//` $\rho_t = \rho(t)$
  if *Dirichlet boundary condition* **then**
    $K_{uu} = K(2:N-1, 2:N-1)$; `// partitioning of matrix` K
    $K_{uk} = [(K(2:N-1,1))^T; (K(2:N-1,N))^T]$;
    $F_u = F(2:N-1,1)$; `// partitioning of vector` F
    $F_k = [F(1,1); F(N,1)]$;
    $\rho_{t+\Delta t}(2:N_\gamma - 1, 1) = \rho_t(2:N_\gamma - 1, 1) + \Delta t (M_{uu}^{-1}(K_{uk}F_k + K_{uu}F_u))$;
    $\rho_{t+\Delta t}(1) = \rho_t(1)$; `// Boundary values are fixed`
    $\rho_{t+\Delta t}(N_\gamma) = \rho_t(N_\gamma)$;
  $\rho_t = \rho_{t+\Delta t}$; `// Iteration`
  $t = t + \Delta t$;

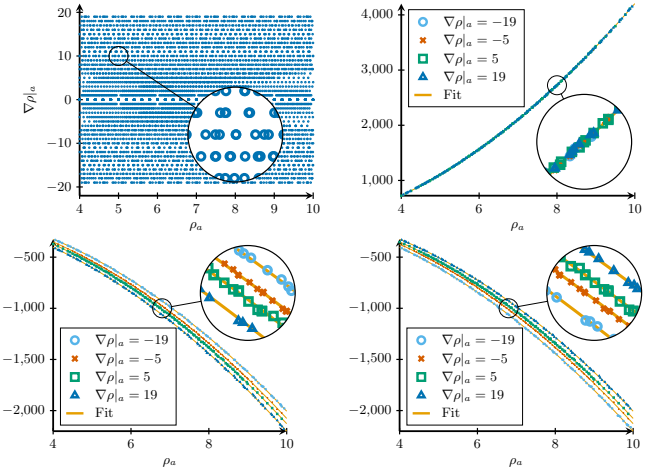

Figure A.6: Data set used in the unconstrained setting. Top left: Discrete set V_{discr} of pairs $(\rho_a, \nabla\rho|_a)$ used to evaluate the discretized operator $\mathcal{K}_\rho$. Remaining plots: Shown are the matrix entries (b, a) of $\langle \mathcal{K}_{(\rho_a + \nabla\rho|_a (x - x_a))} \gamma_a, \gamma_b \rangle$ as function of ρ_a and $\nabla\rho|_a$ for the symmetric zero-range process. The plots are for $a = b$ (top right), $a = b - 1$ (bottom left) and $a = b + 1$ (bottom right). For x, x_a and the profiles γ_a see Fig. 2.

Appendix B. Covariance of the fluctuations

We now provide a proof of the relation

$$\langle \mathcal{K}_z \gamma_a, \gamma_b \rangle = \lim_{h \searrow 0} \frac{1}{2h} \mathbb{E}\Big[\left(Y_{\gamma_a}(t_0 + h) - Y_{\gamma_a}(t_0)\right) \cdot \left(Y_{\gamma_b}(t_0 + h) - Y_{\gamma_b}(t_0)\right) \Big] \tag{B.1}$$

used to compute the discretized operator from the rescaled local fluctuations Y_γ, defined as the stochastic limit of $Y_\gamma^\epsilon = \frac{1}{\sqrt{\epsilon}} \langle z_\epsilon - z, \gamma \rangle$ as $\epsilon \to 0$. The proof follows a similar argument to that in Embacher et al. (2018), where the variation of the fluctuations for a specific operator (the Wasserstein operator) is computed.

From the equations for z_ϵ and $z = \mathbb{E}[z_\epsilon]$, cf. (1) and (2) of the article, the rescaled fluctuations follow

$$\mathrm{d}Y_\gamma = \langle \mathcal{M}_z Y, \gamma \rangle \, \mathrm{d}t + \langle \sqrt{2\mathcal{K}_z} \mathrm{d}W_{x,t}, \gamma \rangle, \tag{B.2}$$

where Y is the limit of $(z_\epsilon - z)/\sqrt{\epsilon}$ and $\mathcal{M}_z$ is a linear operator acting on Y, depending on z, such that $\mathcal{M}_z Y$ is the limit of $\left(\mathcal{K}_{z_\epsilon} DS(z_\epsilon) - \mathcal{K}_z DS(z)\right)/\sqrt{\epsilon}$. Additionally, by Itô's formula, the function $F(X_1, X_2) = (X_1 - Y_{\gamma_a}(t_0))\,(X_2 - Y_{\gamma_b}(t_0))$ satisfies for $X_1 = Y_{\gamma_a}(t)$ and $X_2 = Y_{\gamma_b}(t)$

$$\mathrm{d}F = (Y_{\gamma_b}(t) - Y_{\gamma_b}(t_0))\,\mathrm{d}Y_{\gamma_a} + (Y_{\gamma_a}(t) - Y_{\gamma_a}(t_0))\,\mathrm{d}Y_{\gamma_b} + \langle 2\mathcal{K}_z\gamma_a, \gamma_b\rangle\,\mathrm{d}t. \tag{B.3}$$

Then, the expectation appearing on the right-hand side of (B.1), can be written as

$$\begin{aligned}
&\mathbb{E}\left[(Y_{\gamma_a}(t_0+h) - Y_{\gamma_a}(t_0))\,(Y_{\gamma_b}(t_0+h) - Y_{\gamma_b}(t_0))\right] \\
&= \mathbb{E}\left[F(Y_{\gamma_a}(t_0+h), Y_{\gamma_b}(t_0+h))\right] = \mathbb{E}\left[\int_{t_0}^{t_0+h} \mathrm{d}F\right] \\
&= \mathbb{E}\left[\int_{t_0}^{t_0+h} (Y_{\gamma_b}(t) - Y_{\gamma_b}(t_0))\,\mathrm{d}Y_{\gamma_a}\right] + \mathbb{E}\left[\int_{t_0}^{t_0+h} (Y_{\gamma_a}(t) - Y_{\gamma_a}(t_0))\,\mathrm{d}Y_{\gamma_b}\right] \\
&\quad + \mathbb{E}\left[\int_{t_0}^{t_0+h} \langle 2\mathcal{K}_z\gamma_a, \gamma_b\rangle\,\mathrm{d}t\right].
\end{aligned} \tag{B.4}$$

The sought-after result then immediately follows if

$$\begin{aligned}
\lim_{h\searrow 0} \frac{1}{2h}\mathbb{E}\left[\int_{t_0}^{t_0+h} (Y_{\gamma_b}(t) - Y_{\gamma_b}(t_0))\,\mathrm{d}Y_{\gamma_a}\right] = 0, \\
\lim_{h\searrow 0} \frac{1}{2h}\mathbb{E}\left[\int_{t_0}^{t_0+h} (Y_{\gamma_a}(t) - Y_{\gamma_a}(t_0))\,\mathrm{d}Y_{\gamma_b}\right] = 0,
\end{aligned} \tag{B.5}$$

which we proceed to show.

By Hölder's and Young's inequality

$$\begin{aligned}
&\mathbb{E}\left[\int_{t_0}^{t_0+h} (Y_{\gamma_b}(t) - Y_{\gamma_b}(t_0))\,\mathrm{d}Y_{\gamma_a}\right] \\
&= \mathbb{E}\left[\int_{t_0}^{t_0+h} (Y_{\gamma_b}(t) - Y_{\gamma_b}(t_0))\,\langle \mathcal{M}_z Y, \gamma_a\rangle\,\mathrm{d}t\right] \\
&\leq \sqrt{\mathbb{E}\left[\int_{t_0}^{t_0+h} (Y_{\gamma_b}(t) - Y_{\gamma_b}(t_0))^2\,\mathrm{d}t\right]} \quad \cdot \sqrt{\mathbb{E}\left[\int_{t_0}^{t_0+h} (\langle \mathcal{M}_z Y, \gamma_a\rangle)^2\,\mathrm{d}t\right]} \\
&\leq \frac{1}{2}\int_{t_0}^{t_0+h} \mathbb{E}\left[(Y_{\gamma_b}(t) - Y_{\gamma_b}(t_0))^2\right]\mathrm{d}t + \frac{1}{2}\int_{t_0}^{t_0+h} \mathbb{E}\left[(\langle \mathcal{M}_z Y, \gamma_a\rangle)^2\right]\mathrm{d}t,
\end{aligned} \tag{B.6}$$

and analogously for $\mathbb{E}\left[\int_{t_0}^{t_0+h} (Y_{\gamma_a}(t_0+h) - Y_{\gamma_a}(t_0))\,\mathrm{d}Y_{\gamma_b}\right]$. Next, we define the auxiliary variables

$$\begin{aligned}
Z_j(t) &= \int_{t_0}^{t} \mathbb{E}\left[\left(Y_{\gamma_j}(s) - Y_{\gamma_j}(t_0)\right)^2\right]\mathrm{d}s \quad \text{and} \\
R_j(t) &= \int_{t_0}^{t} \mathbb{E}\left[(\langle \mathcal{M}_z Y, \gamma_j\rangle)^2\right]\mathrm{d}s + \int_{t_0}^{t} \langle 2\mathcal{K}_z\gamma_j, \gamma_j\rangle \mathrm{d}s
\end{aligned} \tag{B.7}$$

with $j = a$ or b. From (B.4), (B.5) and (B.6) for $\gamma_a = \gamma_b = \gamma_j$, it follows that $\dot{Z}_j(t) \leq Z_j(t) + R_j(t)$, with $R_j(t)$ continuous. By Gronwall's lemma

$$Z_j(t) \leq e^{(t-t_0)} \int_{t_0}^{t} e^{-(s-t_0)} R_j(s)\mathrm{d}s, \tag{B.8}$$

and, since $R_j(h) = \mathcal{O}(h)$, $Z_j(t_0 + h) = \mathcal{O}(h^2)$. Then, using the second but last inequality in (B.6),

$$\mathbb{E}\left[\int_{t_0}^{t_0+h} (Y_{\gamma_b}(t) - Y_{\gamma_b}(t_0))\,\mathrm{d}Y_{\gamma_a}\right] = \mathcal{O}(h^{3/2}). \tag{B.9}$$

Similarly,

$$\mathbb{E}\left[\int_{t_0}^{t_0+h} (Y_{\gamma_a}(t) - Y_{\gamma_a}(t_0))\,\mathrm{d}Y_{\gamma_b}\right] = \mathcal{O}(h^{3/2}), \tag{B.10}$$

which leads to (B.5), concluding the proof.

Appendix C. Error in the Taylor expansion of the operator

We now examine the error of the approximation

$$\sum_a \langle \mathcal{K}_\rho \gamma_a, \gamma_b\rangle F_a \simeq \sum_{a\in\{b-1,b,b+1\}} \langle \mathcal{K}_{(\rho_a + \nabla\rho|_a(x-x_a))}\gamma_a, \gamma_b\rangle F_a \tag{C.1}$$

for a diffusion process, i.e., a process with $\langle \mathcal{K}_\rho\gamma_a, \gamma_b\rangle = \langle m(\rho)\nabla\gamma_a, \nabla\gamma_b\rangle$, and linear shape functions.

We begin by computing the three elements of the tridiagonal, using a Taylor expansion of the mobility coefficient m, as in (C.1):

$$\begin{aligned}
\langle m\nabla\gamma_b, \nabla\gamma_b\rangle &= \langle m_b\nabla\gamma_b, \nabla\gamma_b\rangle + \left\langle \frac{\partial m}{\partial x}\Big|_b (x-x_b)\nabla\gamma_b, \nabla\gamma_b\right\rangle \\
&\quad + \left\langle \frac{1}{2}\frac{\partial^2 m}{\partial x^2}\Big|_b (x-x_b)^2\nabla\gamma_b, \nabla\gamma_b\right\rangle + \mathcal{O}(\Delta x^2) \\
&= 2\frac{m_b}{\Delta x} + \frac{1}{3}\frac{\partial^2 m}{\partial x^2}\Big|_b \Delta x + \mathcal{O}(\Delta x^2), \qquad \text{(C.2)} \\
\langle m\nabla\gamma_{b-1}, \nabla\gamma_b\rangle &= \langle m_{b-1}\nabla\gamma_{b-1}, \nabla\gamma_b\rangle + \left\langle \frac{\partial m}{\partial x}\Big|_{b-1} (x-x_{b-1})\nabla\gamma_{b-1}, \nabla\gamma_b\right\rangle \\
&\quad + \left\langle \frac{1}{2}\frac{\partial^2 m}{\partial x^2}\Big|_{b-1} (x-x_{b-1})^2\nabla\gamma_{b-1}, \nabla\gamma_b\right\rangle + \mathcal{O}(\Delta x^2) \\
&= -\frac{m_{b-1}}{\Delta x} - \frac{1}{2}\frac{\partial m}{\partial x}\Big|_{b-1} - \frac{1}{6}\frac{\partial^2 m}{\partial x^2}\Big|_{b-1}\Delta x + \mathcal{O}(\Delta x^2), \qquad \text{(C.3)} \\
\langle m\nabla\gamma_{b+1}, \nabla\gamma_b\rangle &= \langle m_{b+1}\nabla\gamma_{b+1}, \nabla\gamma_b\rangle + \left\langle \frac{\partial m}{\partial x}\Big|_{b+1} (x-x_{b+1})\nabla\gamma_{b+1}, \nabla\gamma_b\right\rangle \\
&\quad + \left\langle \frac{1}{2}\frac{\partial^2 m}{\partial x^2}\Big|_{b+1} (x-x_{b+1})^2\nabla\gamma_{b+1}, \nabla\gamma_b\right\rangle + \mathcal{O}(\Delta x^2) \\
&= -\frac{m_{b+1}}{\Delta x} + \frac{1}{2}\frac{\partial m}{\partial x}\Big|_{b+1} - \frac{1}{6}\frac{\partial^2 m}{\partial x^2}\Big|_{b+1}\Delta x + \mathcal{O}(\Delta x^2), \qquad \text{(C.4)}
\end{aligned}$$

where Δx is the spacing of the macroscopic finite element nodes, and m_b and $\frac{\partial m}{\partial x}\Big|_b$ denote the value of the mobility coefficient and its gradient at x_b. The sum in the right hand side of (C.1) may be most easily expressed by writing the off-diagonal terms as a function of the mobility and its derivative at x_b. Using the

approximations

$$
\begin{aligned}
m_{b-1} &= m_b - \frac{\partial m}{\partial x}\Big|_b \Delta x + \frac{1}{2}\frac{\partial^2 m}{\partial x^2}\Big|_b (\Delta x)^2 + \mathcal{O}(\Delta x^3),\\
m_{b+1} &= m_b + \frac{\partial m}{\partial x}\Big|_b \Delta x + \frac{1}{2}\frac{\partial^2 m}{\partial x^2}\Big|_b (\Delta x)^2 + \mathcal{O}(\Delta x^3),\\
\frac{\partial m}{\partial x}\Big|_{b-1} &= \frac{\partial m}{\partial x}\Big|_b - \frac{\partial^2 m}{\partial x^2}\Big|_b \Delta x + \mathcal{O}(\Delta x^2), \qquad & \frac{\partial m}{\partial x}\Big|_{b+1} &= \frac{\partial m}{\partial x}\Big|_b + \frac{\partial^2 m}{\partial x^2}\Big|_b \Delta x + \mathcal{O}(\Delta x^2),\\
\frac{\partial^2 m}{\partial x^2}\Big|_{b-1} &= \frac{\partial^2 m}{\partial x^2}\Big|_b + \mathcal{O}(\Delta x), & \frac{\partial^2 m}{\partial x^2}\Big|_{b+1} &= \frac{\partial^2 m}{\partial x^2}\Big|_b + \mathcal{O}(\Delta x),
\end{aligned}
$$

the off-diagonal terms (C.3) and (C.4) become

$$
\begin{aligned}
\langle m\nabla\gamma_{b-1}, \nabla\gamma_b\rangle &= -\frac{m_b}{\Delta x} + \frac{1}{2}\frac{\partial m}{\partial x}\Big|_b - \frac{1}{6}\frac{\partial^2 m}{\partial x^2}\Big|_b \Delta x + \mathcal{O}(\Delta x^2),\\
\langle m\nabla\gamma_{b+1}, \nabla\gamma_b\rangle &= -\frac{m_b}{\Delta x} - \frac{1}{2}\frac{\partial m}{\partial x}\Big|_b - \frac{1}{6}\frac{\partial^2 m}{\partial x^2}\Big|_b \Delta x + \mathcal{O}(\Delta x^2).
\end{aligned}
$$

From this and (C.2), the discretization (C.1) becomes

$$
\begin{aligned}
\sum_{a\in\{b-1,b,b+1\}} \langle \mathcal{K}_\rho\gamma_a, \gamma_b\rangle F_a = &\left[2\frac{m_b}{\Delta x} + \frac{1}{3}\frac{\partial^2 m}{\partial x^2}\Big|_b \Delta x\right] F_b\\
&+ \left[-\frac{m_b}{\Delta x} + \frac{1}{2}\frac{\partial m}{\partial x}\Big|_b - \frac{1}{6}\frac{\partial^2 m}{\partial x^2}\Big|_b \Delta x\right] F_{b-1}\\
&+ \left[-\frac{m_b}{\Delta x} - \frac{1}{2}\frac{\partial m}{\partial x}\Big|_b - \frac{1}{6}\frac{\partial^2 m}{\partial x^2}\Big|_b \Delta x\right] F_{b+1} + \mathcal{O}(\Delta x^2).
\end{aligned}
$$

An equivalent expression is obtained by regrouping the terms,

$$
\begin{aligned}
\sum_{a\in\{b-1,b,b+1\}} \langle \mathcal{K}_\rho\gamma_a, \gamma_b\rangle F_a &= -\frac{m_b}{\Delta x}\left(-2F_b + F_{b-1} + F_{b+1}\right) - \frac{1}{2}\frac{\partial m}{\partial x}\Big|_b \left(F_{b+1} - F_{b-1}\right)\\
&\quad - \frac{1}{6}\frac{\partial^2 m}{\partial x^2}\Big|_b \Delta x \left(-2F_b + F_{b-1} + F_{b+1}\right) + \mathcal{O}(\Delta x^2)\\
&= \Delta x\left[-m_b \Delta F|_b - \frac{\partial m}{\partial x}\Big|_b \nabla F|_b\right] - \frac{1}{6}\frac{\partial^2 m}{\partial x^2}\Big|_b \Delta F|_b \,(\Delta x)^3 + \mathcal{O}(\Delta x^2),
\end{aligned}
$$

where $\Delta F|_b = \left(-2F_b + F_{b-1} + F_{b+1}\right)/\Delta x^2$ and $\nabla F|_b = \left(F_{b+1} - F_{b-1}\right)/(2\Delta x)$ denote the discretized Laplacian and gradient at point x_b, which differ from the exact values by errors of the order of Δx^2. The expected right hand side of the discretized PDE is therefore recovered up to errors of the order of Δx^3 (note that the terms $\mathcal{O}(\Delta x^2)$, once combined, actually lead to errors of order Δx^3).

Acknowledgments

All the authors thank the Leverhulme Trust for its support via grant no. RPG-2013-261. J.Z. gratefully acknowledges funding by a Royal Society Wolfson Research Merit Award. P.E. thanks Cardiff University through the International Collaboration Seedcorn Fund to visit C.R.; X.L. and C.R. thank the University Research Foundation Grant from the University of Pennsylvania.

Assyr Abdulle, Weinan E, Björn Engquist, and Eric Vanden-Eijnden. The heterogeneous multiscale method. *Acta Numer.*, 21: 1–87, 2012. ISSN 0962-4929. doi: 10.1017/S0962492912000025. URL `https://doi.org/10.1017/S0962492912000025`.

Thierry Bodineau, Isabelle Gallagher, and Laure Saint-Raymond. The Brownian motion as the limit of a deterministic system of hard-spheres. *Invent. Math.*, 203(2):493–553, 2016. ISSN 0020-9910. doi: 10.1007/s00222-015-0593-9. URL http://dx.doi.org/10.1007/s00222-015-0593-9.

Maria Bruna and S. Jonathan Chapman. Excluded-volume effects in the diffusion of hard spheres. *Phys. Rev. E*, 85:011103, Jan 2012. doi: 10.1103/PhysRevE.85.011103. URL https://link.aps.org/doi/10.1103/PhysRevE.85.011103.

E. Carter, J. E. Taylor, and J. W. Cahn. Variational methods for microstructural-evolution theories. *JOM*, 49(12):30–36, 1997.

Mario Castro. Phase-field approach to heterogeneous nucleation. *Phys. Rev. B*, 67:035412, 2003. doi: 10.1103/PhysRevB.67.035412. URL https://link.aps.org/doi/10.1103/PhysRevB.67.035412.

Bryan C. Daniels and Ilya Nemenman. Automated adaptive inference of phenomenological dynamical models. *Nat. Commun.*, 6:8133 EP, 2015. URL http://dx.doi.org/10.1038/ncomms9133.

David S. Dean. Langevin equation for the density of a system of interacting Langevin processes. *J. Phys. A*, 29(24):L613, 1996. URL http://stacks.iop.org/0305-4470/29/i=24/a=001.

B. Derrida, J. L. Lebowitz, E. R. Speer, and H. Spohn. Dynamics of an anchored Toom interface. *J. Phys. A*, 24(20):4805–4834, 1991. ISSN 0305-4470. URL http://stacks.iop.org/0305-4470/24/4805.

Nicolas Dirr, Marios Stamatakis, and Johannes Zimmer. Entropic and gradient flow formulations for nonlinear diffusion. *J. Math. Phys.*, 57(8):081505, 13, 2016. ISSN 0022-2488. doi: 10.1063/1.4960748. URL http://dx.doi.org/10.1063/1.4960748.

Miguel A. Durán-Olivencia, Peter Yatsyshin, Benjamin D. Goddard, and Serafim Kalliadasis. General framework for fluctuating dynamic density functional theory. *New J. Phys.*, 19(12):123022, 2017. URL http://stacks.iop.org/1367-2630/19/i=12/a=123022.

Peter Embacher, Nicolas Dirr, Johannes Zimmer, and Celia Reina. Computing diffusivities from particle models out of equilibrium. *Proc. Roy. Soc. London Ser. A*, 474(2212), 2018. ISSN 364-5021. doi: 10.1098/rspa.2017.0694. URL http://rspa.royalsocietypublishing.org/content/474/2212/20170694.

Radek Erban, Ioannis G. Kevrekidis, and Hans G. Othmer. An equation-free computational approach for extracting population-level behavior from individual-based models of biological dispersal. *Phys. D*, 215(1):1–24, 2006. ISSN 0167-2789. doi: 10.1016/j.physd.2006.01.008. URL https://doi.org/10.1016/j.physd.2006.01.008.

Gregory L. Eyink. Dissipation and large thermodynamic fluctuations. *J. Statist. Phys.*, 61(3-4):533–572, 1990. ISSN 0022-4715. doi: 10.1007/BF01027291. URL http://dx.doi.org/10.1007/BF01027291.

Gregory L. Eyink, Joel L. Lebowitz, and Herbert Spohn. Hydrodynamics and fluctuations outside of local equilibrium: driven diffusive systems. *J. Statist. Phys.*, 83(3-4):385–472, 1996. ISSN 0022-4715. doi: 10.1007/BF02183738. URL http://dx.doi.org/10.1007/BF02183738.

Dror Givon, Raz Kupferman, and Andrew Stuart. Extracting macroscopic dynamics: model problems and algorithms. *Nonlinearity*, 17(6):R55–R127, 2004. ISSN 0951-7715. doi: 10.1088/0951-7715/17/6/R01. URL http://dx.doi.org/10.1088/0951-7715/17/6/R01.

Melville S. Green. Markoff random processes and the statistical mechanics of time-dependent phenomena. II. Irreversible processes in fluids. *J. Chem. Phys.*, 22:398–413, 1954. ISSN 0021-9606. doi: 10.1063/1.1740082. URL http://dx.doi.org/10.1063/1.1740082.

Stefan Grosskinsky, Gunter M. Schütz, and Herbert Spohn. Condensation in the zero range process: stationary and dynamical properties. *J. Statist. Phys.*, 113(3-4):389–410, 2003. ISSN 0022-4715. doi: 10.1023/A:1026008532442. URL http://dx.doi.org/10.1023/A:1026008532442.

Günther Grün, Klaus Mecke, and Markus Rauscher. Thin-film flow influenced by thermal noise. *J. Stat. Phys.*, 122(6):1261–1291, 2006. ISSN 0022-4715. doi: 10.1007/s10955-006-9028-8. URL http://dx.doi.org/10.1007/s10955-006-9028-8.

P. C. Hohenberg and B. I. Halperin. Theory of dynamic critical phenomena. *Rev. Mod. Phys.*, 49:435–479, 1977. doi: 10.1103/RevModPhys.49.435. URL http://link.aps.org/doi/10.1103/RevModPhys.49.435.

Ioannis G. Kevrekidis and Giovanni Samaey. Equation-free multiscale computation: Algorithms and applications. *Annu. Rev. Phys. Chem.*, 60(1):321–344, 2009. doi: 10.1146/annurev.physchem.59.032607.093610. URL https://doi.org/10.1146/annurev.physchem.59.032607.093610. PMID: 19335220.

Claude Kipnis and Claudio Landim. *Scaling limits of interacting particle systems*, volume 320 of *Grundlehren der Mathematischen Wissenschaften [Fundamental Principles of Mathematical Sciences]*. Springer-Verlag, Berlin, 1999. ISBN 3-540-64913-1.

Rainer Klages, Wolfram Just, and Christopher Jarzynski, editors. *Nonequilibrium statistical physics of small systems*. Reviews of Nonlinear Dynamics and Complexity. Wiley-VCH, Weinheim, 2013. ISBN 978-3-527-41094-1; 978-3-527-65872-5. doi: 10.1002/9783527658701. URL https://doi.org/10.1002/9783527658701. Fluctuation relations and beyond.

R. Kubo. The fluctuation-dissipation theorem. *Rep. Prog. Phys.*, 29(1):255, 1966. URL http://stacks.iop.org/0034-4885/29/i=1/a=306.

Claudio Landim. Hydrodynamic limit of interacting particle models. Lecture Notes, School and Conference on Probability Theory, Trieste 13–31 May 2002, 2002.

Tony Lelièvre, Mathias Rousset, and Gabriel Stoltz. *Free energy computations*. Imperial College Press, London, 2010. ISBN 978-1-84816-247-1; 1-84816-247-2. doi: 10.1142/9781848162488. URL http://dx.doi.org/10.1142/9781848162488. A mathematical perspective.

James F. Lutsko. A dynamical theory of nucleation for colloids and macromolecules. *J. Chem. Phys.*, 136:034509, 2012. doi: 10.1063/1.3677191. URL http://jcp.aip.org/resource/1/jcpsa6/v136/i3/p034509_s1.

Benjamin B. Machta, Ricky Chachra, Mark K. Transtrum, and James P. Sethna. Parameter space compression underlies emergent theories and predictive models. *Science*, 342(6158):604–607, 2013. ISSN 0036-8075. doi: 10.1126/science.1238723. URL http://science.sciencemag.org/content/342/6158/604.

Christian Maes. The fluctuation theorem as a Gibbs property. *J. Statist. Phys.*, 95(1-2):367–392, 1999. ISSN 0022-4715. doi:

10.1023/A:1004541830999. URL http://dx.doi.org/10.1023/A:1004541830999.

Umberto Marini Bettolo Marconi, Andrea Puglisi, Lamberto Rondoni, and Angelo Vulpiani. Fluctuation-dissipation: Response theory in statistical physics. *Physics Reports*, 461(4):111 – 195, 2008. ISSN 0370-1573. doi: https://doi.org/10.1016/j.physrep.2008.02.002. URL http://www.sciencedirect.com/science/article/pii/S0370157308000768.

Helmut Mehrer. *Diffusion in Solids: Fundamentals, Methods, Materials, Diffusion-Controlled Processes*. Springer Series in Solid-State Sciences. Springer, Berlin, Heidelberg, 2007.

Alexander Mielke. Formulation of thermoelastic dissipative material behavior using GENERIC. *Contin. Mech. Thermodyn.*, 23(3):233–256, 2011. ISSN 0935-1175. doi: 10.1007/s00161-010-0179-0. URL http://dx.doi.org/10.1007/s00161-010-0179-0.

Hans Christian Öttinger. *Beyond equilibrium thermodynamics*. Wiley Online Library, 2005.

Maziar Raissi. Deep hidden physics models: Deep learning of nonlinear partial differential equations, 2018.

Celia Reina and Johannes Zimmer. Entropy production and the geometry of dissipative evolution equations. *Phys. Rev. E*, 92 (5):052117, 7, 2015. doi: 10.1103/PhysRevE.92.052117. URL http://link.aps.org/doi/10.1103/PhysRevE.92.052117.

Samuel H. Rudy, Steven L. Brunton, Joshua L. Proctor, and J. Nathan Kutz. Data-driven discovery of partial differential equations. *Sci. Adv.*, 3(4):e1602614, 2017. doi: 10.1126/sciadv.1602614. URL http://www.ncbi.nlm.nih.gov/pmc/articles/PMC5406137/.

Greg J. Stephens, Leslie C. Osborne, and William Bialek. Searching for simplicity in the analysis of neurons and behavior. *PNAS*, 108(Supplement 3):15565–15571, 2011. ISSN 0027-8424. doi: 10.1073/pnas.1010868108. URL http://www.pnas.org/content/108/Supplement_3/15565.

Rouslan L. Stratonovich. *Nonlinear nonequilibrium thermodynamics. I*, volume 57 of *Springer Series in Synergetics*. Springer-Verlag, Berlin, 1992. ISBN 3-540-55216-2. doi: 10.1007/978-3-642-77343-3. URL https://doi.org/10.1007/978-3-642-77343-3. Linear and nonlinear fluctuation-dissipation theorems, Translated from the Russian by V. V. Stratonovich and A. P. Repjev.

Ellad B. Tadmor and Ronald E. Miller. *Modeling Materials: Continuum, Atomistic and Multiscale Techniques*. Cambridge University Press, 2011. doi: 10.1017/CBO9781139003582.

A. G. Thompson, J. Tailleur, M. E. Cates, and R. A. Blythe. Lattice models of nonequilibrium bacterial dynamics. *J. Stat. Mech. Theory Exp.*, (2):P02029, 34, 2011.

D. G. Vlachos and M. A. Katsoulakis. Derivation and validation of mesoscopic theories for diffusion of interacting molecules. *Phys. Rev. Lett.*, 85:3898–3901, 2000. doi: 10.1103/PhysRevLett.85.3898. URL https://link.aps.org/doi/10.1103/PhysRevLett.85.3898.

Robert Zwanzig. *Nonequilibrium statistical mechanics*. Oxford University Press, New York, 2001. ISBN 0-19-514018-4.